

The surface structure of Au(111) in the presence of organic adlayers: a combined electrochemical and surface X-ray scattering study¹

Th. Wandlowski^a, B.M. Ocko^b, O.M. Magnussen^b, S. Wu^c, J. Lipkowski^c

^a Department of Electrochemistry, University of Ulm, D-89069 Ulm, Germany

^b Department of Physics, Brookhaven National Laboratory, Upton, NY, USA

^c Department of Chemistry and Biochemistry, University of Guelph, Guelph, Canada

Received 18 September 1995

Abstract

In situ X-ray scattering studies of the Au(111) electrode surface have been carried out in KClO₄ solutions containing uracil, pyridine or 2,2'-bipyridine using grazing-incident-angle diffraction. At sufficiently negative potentials, the ($p \times \sqrt{3}$) surface reconstruction forms with a stripe separation $p = 23$. The formation of a two-dimensional condensed uracil film or a complete monolayer of planar oriented pyridine or 2,2'-bipyridine hinders the lifting of the reconstruction. Whereas the stripe separation increases continuously over a 0.6 V range in the base electrolyte, the presence of the organic compounds blocks this process considerably. Only a small, step-like increase in p is observed, where the adlayer is disordered. There exists a 0.7 V hysteresis between the lifting and the subsequent formation of the reconstruction. The ($p \times \sqrt{3}$) phase reappears at potentials where a 'gas-like' adlayer is formed once again. Cyclic diffractograms and potential step measurements have been employed to study the time dependence of these substrate transitions for the system uracil|Au(111).

Keywords: X-ray studies; Au(111); Organic adlayers

1. Introduction

It is well established from UHV-studies that all three low-index faces of gold single crystals are reconstructed at room temperature, e.g. the surface atoms acquire positions with a periodicity and symmetry pattern distinctly different from the underlying bulk layers [1–4]. Hamelin suggested the concept of electrochemically-induced reconstruction in order to explain the hysteresis in the capacitance vs. potential curves and certain features in cyclic voltammograms of single crystal gold electrodes in contact with different aqueous electrolyte solutions [5]. This hypothesis was proven by combined electrochemical, in situ electroreflectance spectroscopy and ex situ electron diffraction studies with emersed electrodes by Kolb and co-workers [6–9]. These studies showed that the reconstructed surface structure of the low-index gold single crystal electrodes

can be preserved in situ when the potential is sufficiently negative of the potential of zero charge. The unreconstructed surface is formed when the potential is changed towards sufficiently positive values irrespective of the anion or cation species. The potential (charge) dependence of the gold surface structure and the dynamics involved in the transitions have important consequences for 'true' thermodynamic studies of neutral (organic) and ionic adlayers.

An atomistic picture of the electrode interface has recently emerged with the development of in situ structural methods. Scanning tunneling microscopy (STM) and surface X-ray scattering (SXS) studies carried out under acidic [10–17], basic [18] and neutral [19,20] conditions, all indicate that the atomic structure depends on the potential/charge and that the transition between the reconstructed and the bulk terminated surface is hysteretic. The latter effect was also detected in experiments employing second harmonic generation [21].

For the Au(111) electrode there is a potential (charge) dependent transition between the unreconstructed (1×1) and a striped phase. The striped phase is referred to as a

¹ This paper is based on a presentation given at the Snowdonia Conference on Electrified Interfaces, Harlech, Wales, UK, 17–21 July 1995.

($p \times \sqrt{3}$) structure since it forms a rectangular unit cell with sides p and $\sqrt{3}$ in units of the nearest neighbour gold spacing. X-ray measurements by Wang and coworkers have shown that the stripe separation p is potential dependent and reaches its minimum value $p = 23$ for all electrolyte systems at sufficiently negative potentials [19]. With STM, the uniaxial compression gives rise to a 'double stripe' pattern with a periodicity of about 6.4 nm and a corrugation height of about 0.02 nm [17]. This structure is completely lifted at positive charge densities. Depending on the nature of the applied electrical perturbation (slow scan, potential step), the extra amount of surface atoms from the more densely packed ($p \times \sqrt{3}$) phase will be incorporated into steps and/or form monatomic high islands. The mobility of steps and islands is facilitated by strongly adsorbing anions [22]. STM studies showed further that the transitions between Au(111)–($p \times \sqrt{3}$) and Au(111)–(1 × 1) are most probably controlled by heterogeneous nucleation at defect sites and a rather complicated growth mechanism along the reconstruction elements [16,23].

Despite this progress, the driving force for the electrochemically-induced reconstruction is not fully understood. Systematic SXS studies of the Au(111) electrode in 0.1 M solutions of NaF, NaCl and NaBr suggest that the reconstruction starts to lift at a negative surface charge density of $(-10 \pm 5) \mu\text{C cm}^{-2}$ [19]. These measurements, however, are affected by the specific adsorption of anions, thus it is difficult to ascertain the relative roles of charge and adsorption in determining the phase behaviour. Our study of Au(111) in the presence of organics was partially motivated by the desire to modify the role of adsorption by introducing neutral adsorbates.

Here we report detailed in situ X-ray scattering and electrochemical results from the Au(111) surface in the presence of uracil. SXS is ideally suited to investigate the surface reconstruction in the presence of an adlayer since it is sensitive to both the surface structure and the near surface region. The choice of uracil as a model compound is based on a recent electrochemical and STM study which showed a series of structural transformations [24]. However, the surface coordination of uracil with the underlying gold substrate at high potentials makes it still difficult to determine accurately the 'free surface charge' in the potential region where the reconstruction lifts. Additional measurements of the Au(111) surface, carried out in solutions containing pyridine or 2,2'-bipyridine, exhibit similar potential dependencies as those of uracil. In particular, the large hysteresis between the lifting and the formation of the reconstruction is universal for all three organic molecules investigated.

The paper is organized as follows. In Section 2 we describe some experimental details. The results of the surface X-ray diffraction study are reported in Section 3. The structural and kinetic data of Au(111) surfaces in the presence of uracil will be compared with those obtained

for pyridine, 2,2'-bipyridine and halide anions. A summary of these findings is given in Section 4.

2. Experimental

The electrochemical measurements were carried out with Au(111) single crystal cylinders (4 mm diameter and 4 mm thickness) employing the so-called 'hanging meniscus technique' [25]. Gold-disk electrodes (10 mm diameter, 2 mm thickness), well-aligned along the (111) direction were used in the X-ray measurements. Before each experiment the electrode was annealed until the crystal glowed red for about 2 min. After a short cooling period in air (several minutes), the electrode was quenched in 'Milli-Q' water. The crystal was then transferred to the electrochemical or X-ray cell (for details see Ref. [19]) with a droplet of water adhering to the polished surface. Contact with the electrolyte was established under potential control (at $E = -0.60$ V vs. SCE) in most of the experiments. In the electrochemical measurements a saturated calomel electrode (SCE) was used as a reference, while a Ag|AgCl|KCl(sat) electrode was used for the X-ray measurements. All potentials cited subsequently refer to the Ag|AgCl electrode if not stated otherwise.

The solutions were prepared from 'Milli-Q' water, KClO_4 (Fluka, puriss, p.a.) and various additions of twice recrystallized uracil (Fluka, p.a.), pyridine (Merck, puriss.) or 2,2'-bipyridine (Fluka, p.a.). They were deaerated with 99.999% nitrogen prior to each experiment. Nitrogen was passed over the electrolyte in case of the electrochemical measurements or through the outer chamber of the X-ray cell in order to keep the cell atmosphere free of oxygen. All experiments were carried out at room temperature, $(20 \pm 1)^\circ\text{C}$.

The capacitance measurements were performed using an 18 Hz sine wave of 10 mV (peak-to-peak) amplitude superimposed on a voltage ramp or step. A positive feedback was used to compensate for the solution resistance. The alternating current was amplified by a lock-in amplifier (ITHACO 393). The digitized out-of-phase and in-phase components of the electrode admittance were analysed using a parallel RC equivalent circuit. Other details of the electrochemical measurements are described in Ref. [24].

The X-ray scattering measurements were carried out with focused monochromatic radiation ($\lambda = 1.54 \text{ \AA}$) at the beam line X22B of the National Synchrotron Light Source at Brookhaven National Laboratory. The sample was oriented on a four circle goniometer through its Euler angles θ , χ and ϕ . In order to describe the scattering wave vector (H, K, L) in terms of its components within the surface plane and along the surface normal, a hexagonal coordinate system was employed [19]. The hexagonal reciprocal space lattice constants are $a^* = b^* = 4\pi/a\sqrt{3} = 2.52 \text{ \AA}^{-1}$ and $c^* = 2\pi/a\sqrt{6} = 0.89 \text{ \AA}^{-1}$, where $a = 2.885$

Å is the gold nearest neighbour spacing. The corresponding angles are $\alpha = \beta = 90^\circ$ and $\gamma = 120^\circ$. Further information of the X-ray set-up and the procedures are given in Ref. [19].

3. Results and discussion

3.1. The Au(111) surface in the presence of uracil

3.1.1. Electrochemical data

Fig. 1 shows a typical cyclic voltammogram and the corresponding ‘capacitance’ (actually the frequency-normalized out-of-phase component of the interfacial admittance $Y''/j\omega$) vs. potential curve for Au(111) in 50 mM KClO₄ containing 12 mM uracil [24]. Four different potential regions, labelled I to IV in Fig. 1, may be distinguished.

Region I: This is assigned to the random adsorption of uracil molecules. The adsorbate coverage is increasing

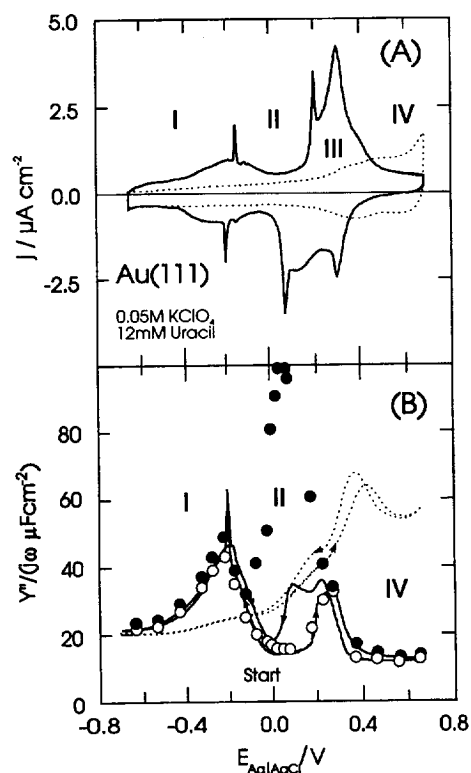


Fig. 1. (A) Current–potential and (B) frequency normalized out-of-phase component of the interfacial admittance for Au(111) in 50 mM KClO₄ in the absence (-----) and in the presence (—) of 12 mM uracil at 20°C. Scan rate 10 mV s⁻¹. The $Y''/j\omega$ curve in the presence of uracil was always composed of two traces. The electrode was immersed under potential control at $E = 0.05$ V. After a waiting time long enough to establish a steady state the potential was either scanned towards positive or negative values, and subsequently reversed. Some data of potential step experiments are added. The filled and open circles in (B) correspond to the initial ($t \rightarrow 0$) and final ($t \rightarrow \infty$) values of $Y''/j\omega$ obtained after the application of a single potential step from $E_i = 0.50$ V and E_f variable.

continuously from -0.75 V (complete desorption) up to approximately -0.2 V.

Region II: Current spikes, which exist in the positive scan direction of the voltammogram at -0.17 V and at 0.20 V, indicate two-dimensional phase transitions. They represent the formation and dissolution of an ordered uracil adlayer respectively (Fig. 1(A)). The molecules are physisorbed on the gold surface and most probably planar oriented [24]. This phase is labelled region II.

We note that the positions of the transition peaks in the subsequent negative scan are significantly shifted towards more negative potentials. The voltammetric features have their counterparts in sharp discontinuities in the corresponding ‘capacitance’ vs. potential curves (Fig. 1(B)), which delimit the so-called ‘pit’ region II [24]. The pit width decreases with increasing uracil concentration and increasing temperature. Phase II exists only at adsorbate concentrations greater than 2 mM and is stable at temperatures as high as 60°C. A marked, but distinctly different hysteresis is observed at both edges of region II when changing the direction of the potential scan. Current transients revealed that the features at the negative pit edge, around -0.20 V, are controlled by the kinetics of nucleation and growth of the ordered adlayer II. The nature of the broad hysteresis at the positive stability limit of the condensed uracil film, between 0.0 V and 0.20 V, could not be resolved unambiguously with classical electrochemical measurements.

Region III: The dissolution of the ordered uracil adlayer II at $E > 0.20$ V is followed by a broad peak in the voltammogram (region III). The latter consumes approximately a charge of $60 \mu\text{C cm}^{-2}$ regardless of the uracil concentration. Tentatively, we associate region III with the reorientation of the adsorbate and the formation of a surface coordination compound between uracil and gold surface adatoms. This transition region exhibits marked kinetic control. An example is given in Fig. 1(B), which also shows the initial (just after application of the potential step, $t \rightarrow 0$, filled circles) and final values ($t \rightarrow \infty$, open circles) of $Y''/j\omega$ when stepping the potential from $E_i = 0.50$ V towards more negative values.

Region IV: A new steady state adsorption phase, which is labelled region IV, is formed in $0.35 \text{ V} < E < 0.75 \text{ V}$. This region is characterized by a capacitance of approximately $14 \mu\text{F cm}^{-2}$, which is independent of temperature, potential and adsorbate concentration. The layer shows typical characteristics of a chemisorbed phase. It is, for instance, stable at temperatures as high as 100°C. In situ STM measurements revealed an ordered hexagonal structure with a lattice constant of $(4.7 \pm 0.3) \text{ \AA}$ [24,26]. Interpretation of the observed contrast pattern in geometrical terms gives an area per molecule of $(19 \pm 3) \text{ \AA}^2$. The corresponding values of the surface excess and the uracil coverage amount to $(8.7 \pm 1.5) \cdot 10^{-10} \text{ mol cm}^{-2}$ and 0.38 referring to the underlying gold substrate respectively. The data point to a perpendicular orientation of the uracil

molecule coordinated with the gold surface via the N1 ring-nitrogen. This interpretation is also supported by the structure of coordination complexes of Au(III) and uracil as obtained in crystallographic experiments [27].

The combined charge balance of regions III and IV (q as obtained by integration of the corresponding current in the voltammogram that is plotted in Fig. 1(A)) provides an estimate of the number of electrons n involved in the formation of the steady state chemisorbed phase IV: $n = 0.7$ was calculated with $q = nF\Gamma$, where Γ is the surface excess and F is the Faradaic constant.

The previous discussion showed that the phase behaviour of uracil on Au(111) is rather complicated and that classical electrochemical measurements do not allow one to distinguish between dynamic effects originating from adlayer changes or substrate modifications. Therefore, we explore in the following sections the influence of uracil on the reconstruction phenomena of Au(111) using surface X-ray diffraction. Our focus will be the stability range of the reconstructed Au(111) surface in the presence of the organic molecule and its influence on the potential-induced reconstruction. The results will provide an important guideline for subsequent thermodynamic and kinetic studies on uracil and related compounds, especially in the regions II and IV.

3.1.2. Surface X-ray diffraction experiments

3.1.2.1. Stability of the $(p \times \sqrt{3})$ reconstruction in the presence of uracil.

The Au(111) surface reconstruction is characterized by a small uniaxial compression of the top layer of gold atoms. In terms of a real space unit cell, the reconstruction is referred to a $(p \times \sqrt{3})$ structure, since in the incommensurate direction there is an extra row of surface gold atoms for every p underlying gold rows and in the orthogonal direction the surface gold atoms are commensurate along the $\sqrt{3}$ direction. The $(p \times \sqrt{3})$ -reconstruction gives rise to additional in-plane superstructure reflections beyond the underlying (1×1) signal. Owing to the three symmetry equivalent reconstruction domains (rotated from each other by 120°), the additional reflections are arranged in a hexagonal pattern surrounding the integer (H, K) positions [4,19,20]. For illustrative purposes, the reciprocal space pattern of the Au(111) surface around the low-order diffraction spot $(0,1)$ at $L = 0.5$ is reproduced from Ref. [19] in Fig. 2. The length of the reconstructed superstructure (stripe separation p) is inversely proportional to the incommensurability, $\delta = (\sqrt{3}/2)/p$. By following the intensity and the positional changes of the superstructure reflections with potential the reconstruction of Au(111) can be monitored in situ.

To characterize the reconstructed phase, the scattering profiles are measured through the $(0,1)$ bulk reflection and one of the two surface reflections with the largest wave-vector transfer with $L = 0.2$. The scan is indicated by q_r in

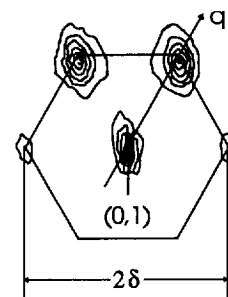


Fig. 2. Schematic representation of the reciprocal space pattern for the Au(111) surface around the low-order bulk-reflection $(0,1)$ at $L = 0.5$. The four satellite spots originate from the $(p \times \sqrt{3})$ reconstructed phase with its three rotationally equivalent domains. The axis q_r is defined to be along the $[1,1]$ direction. The figure is reproduced from Ref. [19].

Fig. 2, where the corresponding in-plane projection is given by $(q_r/\sqrt{3}a^*, 1 + q_r/\sqrt{3}a^*)$. We present in Fig. 3 a typical set of scattering profiles along q_r for 12 mM uracil in 50 mM KClO_4 , after background subtraction. The potential was varied from -0.80 V to 0.70 V and then back to -0.80 V in increments of 50 mV steps. Every fourth profile is plotted in Fig. 3. Each datum point was obtained by counting the scattered intensity for 2 s. The 'effective scan rate' was 0.25 mV s^{-1} . We observed that

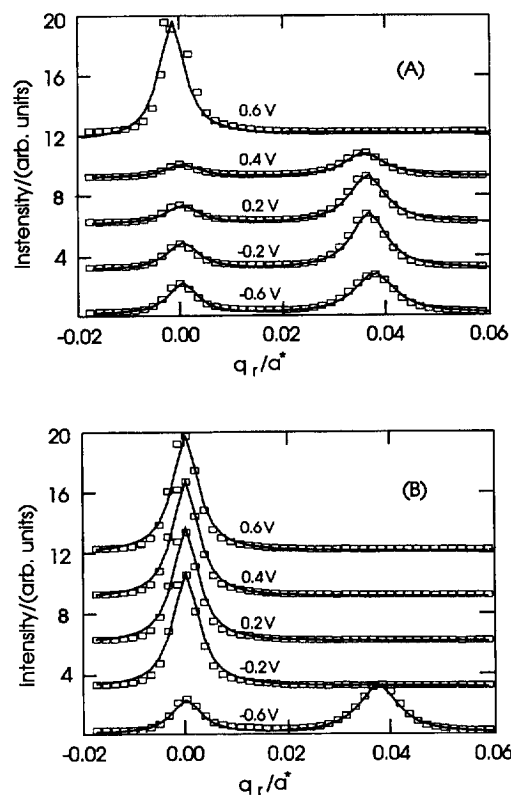


Fig. 3. Typical set of the X-ray diffraction profiles along the q_r axis at $L = 0.2$ for 12 mM uracil at the 50 mM $\text{KClO}_4|\text{Au}(111)$ interface. (A) and (B) represent the positive and negative-going directions of the 'staircase-like' potential scan. The solid lines are fits to a Lorentzian line-shape (Eq. (1)) as described in the text. Subsequent curves are plotted with an offset of 3 units in our scale.

the intensity of the reconstruction peak decreases with increasing potential until it merges at $E \approx 0.60$ V with the diffuse scattering originating from the electrolyte and the window. The reconstruction peak re-emerges after changing the direction of the potential scan, at $E \leq -0.20$ V (Fig. 3(B)), i.e. significant hysteresis occurs. Similar trends can be monitored by following the intensity of the (0, 1) reflection.

A quantitative description has been obtained by fitting the scattering profiles along q_r (see Fig. 3) to the sum of two Lorentzians and a small linear background.

$$I(q_r) = \frac{I_0}{1 + (q_r/a^*)^2/\sigma^2} + \frac{I_\delta}{1 + (q_r/a^* - \delta)^2/\sigma_\delta^2} + A + Bq_r/a^* \quad (1)$$

The first term describes the scattering around (0,1), the second one corresponds to the scattering centered at $(\delta/\sqrt{3}, 1 + \delta/\sqrt{3})$, and A and B are background parameters. The parameters I_0 and I_δ represent peak intensities at $q_r = 0$ and $q_r = \delta a^*$. The stripe separation is given by $L_\delta = pa = a\sqrt{3}/(2\delta)$. σ and σ_δ are respectively the corresponding Lorentzian profile widths, which are measures of the average minimum distance between steps (about 300 Å), and the distance over which atoms in the reconstructed layer are positionally correlated.

For a freshly annealed reconstructed surface we estimate a correlation length of approximately $56a$ at potentials $E \leq -0.60$ V and in the absence of uracil, which is in reasonable agreement with previously estimated data for different inorganic supporting electrolytes [19]. Fig. 4 summarizes the results of the fit in the pure supporting electrolyte (50 mM KClO_4) and with the addition of 12 mM uracil. The stripe separation is shown in (A), the (1×1) intensity is shown in (B), and the integrated intensity ($\sigma_\delta I_\delta$) in (C). The intensities have been normalized to their maximum values.

The maximum compression of the reconstructed surface corresponds to a stripe separation $L_\delta = 23a$. This has been observed in vacuum and under a variety of electrochemical conditions. As shown in Fig. 4(A), the potential-induced reconstructed surface in perchlorate and with the addition of uracil also reaches $L_\delta = 23a$ at about $E \leq -0.60$ V. Subsequently, as long as the potential is kept below -0.30 V, the stripe separation remains fixed at this value. For the pure supporting electrolyte there is a continuous increase in L_δ with increasing potential. At -0.30 V L_δ starts to increase from $23a$, and by 0.30 V it reaches $33a$. Above 0.30 V the reconstruction peak is sufficiently broad that it is difficult to locate its position; correspondingly, L_δ is poorly defined and not shown in Fig. 4(A) at these potentials. However, the integrated reconstructed intensity does not vanish until about 0.45 V. By 0.55 V the (0,1,0,2) intensity reaches its plateau (Fig. 4(B)), and this signifies that the (1×1) surface has fully stabilized. The onset of the transition from the $(23 \times \sqrt{3})$ surface phase to an

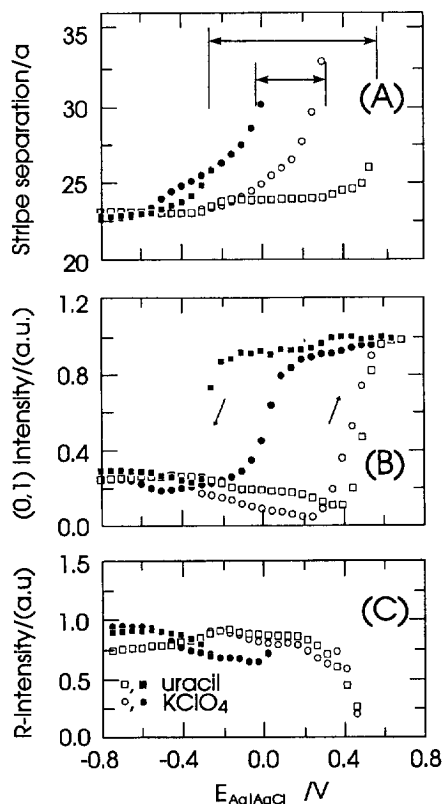


Fig. 4. Stripe separation (A), fitted (0,1) intensity (B) and integrated reconstruction intensity (C) as a function of the electrode potential for 50 mM $\text{KClO}_4|\text{Au}(111)$ in the absence (\circ , \bullet) and in the presence (\square , \blacksquare) of 12 mM uracil. The data have been obtained by fitting Eq. (1) to the scattering profiles (cf. Fig. 3). The open (filled) symbols represent the positive (negative) direction of the potential scan.

ideally terminated surface corresponds approximately to a charge density range between $-10 \mu\text{C cm}^{-2}$ to $-15 \mu\text{C cm}^{-2}$. Similar findings have been obtained for other weakly adsorbing supporting electrolyte systems [19].

The potential range where the reconstruction intensity approaches zero and the (0,1) signal reaches its maximum ($E \approx 0.400$ V) coincides with the detection of monatomic high gold islands with STM [15] and an increase of the surface diffusion coefficient of gold atoms in perchloric acid [28].

The continuous change in L_δ , observed in the pure electrolyte over a wide potential range (see Fig. 4(A), circles), is not observed in the presence of uracil (squares). In the presence of uracil, however, there is a step-like increase in L_δ to $24a$ at about -0.25 V. This potential is close to the transition between randomly adsorbed uracil molecules (region I) and the physisorbed condensed film (region II). Between -0.20 V and 0.30 V (regions II, III and partially IV) L_δ remains constant at $24a$. Furthermore, time-dependent experiments illustrate that this diffraction pattern is stable for hours. Thus, the ordered layer of uracil appears to hinder the mobility of the gold surface atoms, hence stabilizing the reconstruction. But already within the stability region of the chemisorbed film IV (cf. Ref. [24]),

at $E \approx 0.50$ V, L_δ increases abruptly within a narrow potential window (Fig. 4(A)). Simultaneously, the reconstruction intensity approaches zero, and the (0,1,0,2)-signal starts to increase. The scattering intensity at (0,1,0,2) levels off at $E \approx 0.60$ V, where the unreconstructed Au(111)-(1 × 1) surface is completely established. The transition is much more rapid relative to the pure KClO₄-Au(111)-system. The subsequent potential scan towards negative potentials illustrates that the non-reconstructed Au(111) surface is temporarily stable up to -0.30 V in the presence of uracil. This range is much wider than for KClO₄ alone, but also with respect to halide solutions [19].

Complementary information on the Au(111) surface has been obtained by investigating the potential dependence at fixed positions along the specular axis. Previously, it was shown that scattering in the wings of the specular Bragg peaks is sensitive to the density and interlayer expansion, and that changes in these quantities can be monitored at fixed specular positions close to Bragg peaks [10]. In the present hexagonal coordinate system the first specular peak is at (0,0,3) and this corresponds to the (111) reflection in the cubic system. The increase in the top layer spacing which accompanies the formation of the reconstructed surface gives rise to a decrease in the reflectivity at (0,0,3,4) [19]. Conversely, the contraction of the top layer spacing which accompanies the lifting of the reconstruction gives rise to an increase in the reflectivity at (0,0,3,4). As shown in Fig. 5, the specular reflectivity at (0,0,3,4) stays practically constant during the positive scan between $-0.80 \leq E \leq 0.40$ V and corresponds to about 70% of its maximum value. Comparison with Figs. 4(A) and 4(B) shows that the onset of the lifting of the reconstruction causes an increase of the (0,0,3,4) signal. The plateau of the reflectivity at (0,0,3,4) is reached at $E \geq 0.60$ V, which is slightly more positive than the disappearance of the reconstruction peak ($\delta/\sqrt{3}, 1 + \delta/\sqrt{3}, 0, 2$) (Fig. 4). The former may be associated with the formation of detectable monatomic gold islands and with their relax-

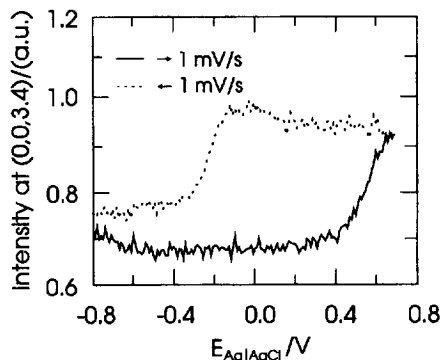


Fig. 5. Potential dependence of the X-ray scattering density for 12 mM uracil in 50 mM KClO₄ | Au(111) at the reciprocal space position (0,0,3,4). The scan rate was 1 mV s⁻¹. The potential scan starts at $E = -0.80$ V. The intensities are normalized to unity at their maximum after background subtraction.

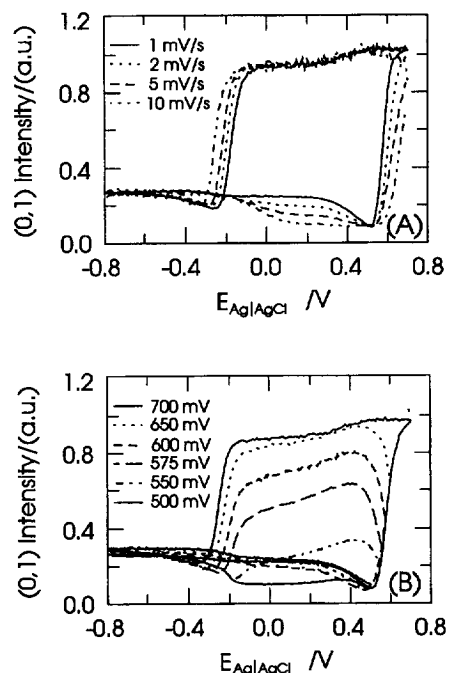


Fig. 6. Potential dependence of the scattering intensity at (0, 1, 0, 2) for 12 mM uracil in 50 mM KClO₄ | Au(111). (A) illustrates the effect of the scan rate and (B) shows the role of the positive return potential. The initial potential was always -0.80 V.

ation dynamics (Ostwald-ripening, merging of equal-sized islands) during the slow-scanning experiment at sufficiently positive potentials [17]. Reversing the potential scan illustrates that the decrease of the (0,0,3,4)-intensity correlates with the reappearance of the reconstruction peak (Fig. 4(C)), which points to the formation of the top gold layer reconstruction.

Effects due to surface disorder can be conveniently studied by monitoring the non-specular intensity in the (0,1,0,2) position [19]. Fig. 6(A) illustrates the scan-rate dependence for $-0.80 \leq E \leq 0.70$ V. The magnitude of the (0,1) signal changes only slightly during the positive potential scan until the detectable lifting of the reconstruction starts, where it first decreases and then increases. This characteristic dip is paralleled by a step-like increase of the stripe separation (Fig. 4(A)) and reflects an increased surface disorder during the lifting of the reconstructed phase. The subsequent increase of the (0,1) intensity at more positive potentials reflects the formation of large patches of the ordered (1 × 1) phase, which is kinetically controlled. Changing the return potential successively towards more negative values shows that the onset of the reordering process requires the passage of a potential threshold E_T , which may be interpreted as the formation of at least one "critical nucleus" of the new substrate phase. The potential corresponds approximately to 0.50 V under the present experimental conditions (Fig. 6(B)). Below E_T , no increase of the (0,1) signal occurs during the reverse potential scan. Above E_T , the (0,1) intensity is

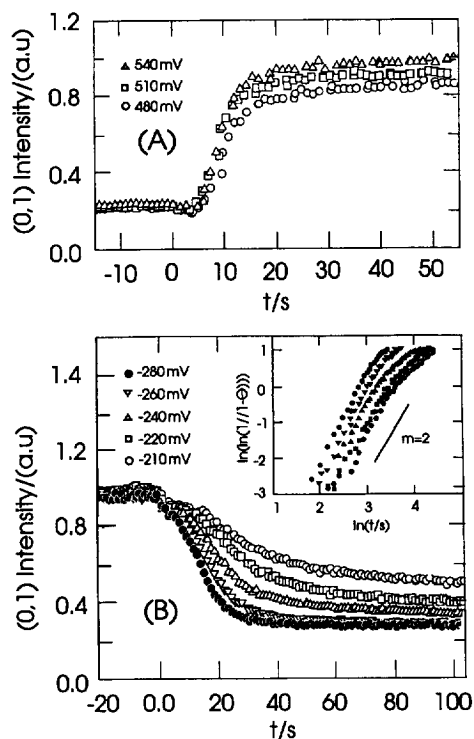


Fig. 7. (A) Time dependence of the (0,1,0,2) intensity after the application of a single potential step towards positive values. The initial potential was $E_i = -0.80$ V and has been applied 5 min before each subsequent potential step. Concentrations are the same as in Fig. 1. (B) Time dependence of the (0, 1, 0, 2) intensity after a potential step from $E_i = 0.70$ V ($t_u = 5$ min) to various final potentials into the stability region of the reconstructed ($p \times \sqrt{3}$) phase. The inset shows the corresponding Avrami-plot.

increasing, which reflects the growth of previously formed nuclei. We also note that the growth proceeds even under conditions which are no longer favourable for the onset of the nucleation. Once formed, the unreconstructed Au(111)–(1×1) surface is rather stable in the presence of uracil up to approximately -0.20 V. This finding is substantiated by the analysis of the scattering profiles described in Figs. 3 and 4.

3.1.3. The kinetics of the $(23 \times \sqrt{3}) \rightleftharpoons (1 \times 1)$ phase transition in the presence of uracil

While the transition between the (1×1) and the reconstructed phase proceeds over a broad potential range for the 50 mM KClO_4 pure supporting electrolyte system (cf. also Ref. [15]), a more rapid transition occurs in the presence of uracil. This finding motivated single-potential step experiments in which the time dependence of the intensity at (0,1,0,2) provides a measure of the surface disorder associated with the phase formation. Fig. 7(A) shows the time dependence of the lifting of the reconstruction in the presence of uracil. The waiting time at $E_i = -0.80$ V was chosen to be long enough so that the surface reconstruction is fully formed and so that there is no organic material adsorbed. As shown in Fig. 7(A), there is

an initial decrease of the (0,1,0,2) intensity during the first 5 s after the application of the potential step, which is followed by a monotonic increase of the signal until a steady state value is reached. The initial decay is not caused by the time-constant of the cell [19] but rather reflects the disordering of the gold surface due to the lifting of the reconstruction ('dip'), which is followed by the formation of an ordered (1×1) top-layer. The complexity of the transient response did not allow us to derive an appropriate mathematical model.

Careful STM studies at the Au(111) surface showed that during the initial stages of the lifting of the ($p \times \sqrt{3}$) reconstruction excess gold atoms are incorporated into steps. Islands are formed at more positive potentials owing to the restrictions of the surface mobility of the gold atoms [16]. Their dynamics in the presence of organics are still poorly understood.

The time dependence of the formation of the reconstruction in the presence of uracil is shown in Fig. 7(B). Starting from a well-ordered (1×1) phase ($E_i = 0.70$ V, $t_i = 5$ min) we observed sigmoid transients for final potentials $E_f \leq -0.10$ V. The (0,1,0,2) intensity decreases faster when choosing more negative potentials for E_f . This observation differs from reports for solutions which contained only halide ions [18]. We applied an Avrami-type of formalism [29,30] to model the transients of Fig. 7(B). Here we have assumed that there is a one-step transition between the (1×1) surface and the ($p \times \sqrt{3}$) reconstructed surface:

$$\theta = 1 - \exp(-b_f t^m) \quad (2)$$

with

$$\theta = [I_{0,1}(t=0) - I_{0,1}(t)] / [I_{0,1}(t=0) - I_{0,1}(t=\infty)] \quad (3)$$

b_f is an apparent rate coefficient and m reflects the dimensionality and the formal nature of the nucleation process. The numerical analysis of our data yields straight lines when plotting $\ln(-\ln(1/(1-\theta)))$ vs. $\ln t$, with a slope m ranging between 1.9 and 2.3. Deviations from linearity occur at larger values of θ , close to the completion of the transition. The more detailed interpretation of the power law dependence is not very meaningful at this stage owing to the complex nature of the (0,1) intensity. Comparative studies with other systems should allow further insight.

3.2. Comparison of the Au(111) surface in the presence of different organic adsorbates

Our uracil study is complemented by selected experiments with pyridine and 2,2'-bipyridine in 50 mM KClO_4 . Fig. 8 shows the stripe separation and the integrated reconstruction intensity for all three organic molecules based on an analysis of the scattering profiles along the q_x axis. For comparison, we added the corresponding set of charge density vs. potential curves, which have been ob-

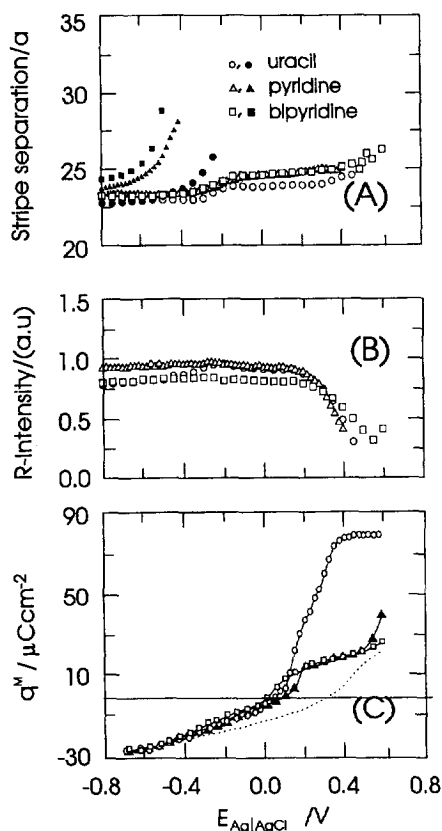


Fig. 8. Stripe separation (A), integrated reconstruction intensity (B) and charge density (C) as a function of potential for 50 mM $\text{KClO}_4|\text{Au}(111)$ in the presence of 12 mM uracil (\circ , \bullet), 10 mM pyridine (Δ , \blacktriangle) and 10 mM 2,2'-bipyridine (\square , \blacksquare). The data have been obtained by fitting the X-ray scattering profiles along q_r (A, B), or from a set of chronocoulometric step-experiments (C). The open (filled) symbols represent the positive (negative) direction of the potential scan.

tained from chronocoulometric measurements [31–33]. Starting the scanning experiment at negative potentials ($E_i = -0.80$ V) the reconstructed ($p \times \sqrt{3}$) gold surface is stabilized up to 0.40 V, rather independent of the charge density or the organic molecule studied. We note that the step-like increase of the stripe separation at $E \approx -0.20$ V corresponds to the formation of a complete monolayer of planar oriented pyridine, 2,2'-bipyridine or a 2D-condensed film composed of a hydrogen-bonded network of uracil [24]. All molecules coordinate with their π -bonds to the substrate surface at negative charge densities. The attractive lateral interactions within the adlayer obviously prevent surface gold atoms from leaving the reconstructed top substrate layer. It is not clear if this effect is controlled by slow kinetics or purely by thermodynamics.

With increasing coverage and potential all species studied undergo an orientational transition, which is completed with the formation of highly ordered structures (cf. STM image of region IV for uracil in Ref. [24]) at the positively charged interface. The (chemisorbed) structures are probably stabilized by an N-bonded coordination between one of the nitrogen atoms of the molecule and the metal surface.

(There is, for instance, a significant partial charge transfer of approximately 0.7 electrons per molecule for uracil in regions III and IV [24].) Sette et al. showed that the formation of an ionic or covalent adsorbate–metal bond should weaken the interlayer and intralayer metal–metal bonds [34], which, in principle, favours the lifting of the surface reconstruction. Such a situation is typical for the halide-induced lifting of the reconstruction of Au(111) [19] and of Au(100) [7] where the metal–metal bond-weakening is not superimposed by the presence of an ordered adlayer on top of it. The ‘charge-density’-induced formation of the unreconstructed Au(111)–(1 × 1) structure takes place under conditions where the halide ions (atoms) form a rather mobile, highly disordered ‘gas-like’ adlayer (the halide coverage is less than 10%), which is characterized by repulsive lateral interactions [19,34–36]. In the case of the present organic molecules (uracil, pyridine, 2,2'-bipyridine) highly organized adlayer structures are formed by lateral attractive interactions [24,31,32], which may compensate the unfavourable metal–metal bond weakening due to the chemisorption up to a critical threshold. The kinetics of the ($p \times \sqrt{3}$) → (1 × 1) transitions are determined by the ability to form critical nuclei of the new phase and the mobility of the ‘freed’ gold atoms. The latter is influenced by the stability of the coordination between gold atoms and the N-heterocycles [26,37]. Mobility reasons are probably also responsible for the strong hysteresis in forming the reconstruction once again after reversing the potential towards more negative values. The stripe separation decreases and the reconstruction intensity increases at potentials, where the 2D-condensed uracil film dissolves (therefore the kinetics of this system could be followed very clearly) or pyridine and 2,2'-bipyridine form a dilute ‘gas-like’ adsorption layer just before complete desorption.

4. Conclusion

During the last several years our understanding of electrochemically-induced surface reconstructions on the low index faces of gold has vastly improved, yet a complete understanding of the microscopic mechanisms has yet to emerge. Surface charge and adsorption have been postulated as the driving forces for the lifting of the reconstruction. It is important to point out that the gold surfaces form the vacuum-type reconstructions only when the surface is negatively charged. Sufficient positive charging promotes the unreconstructed surface. These facts suggest that the sign of the surface charge plays a distinct role in determining the structure of the top gold layer. This has been supported by theoretical calculations which suggest that an excess surface electron density promotes the formation of the reconstructed surface. Furthermore, it has been shown that the reconstruction starts to lift at a charge density of $(-10 \pm 5) \mu\text{C cm}^{-2}$ in halide-containing electrolyte solu-

tions [19]. Whereas the data are tantalizingly suggestive that the surface charge is the driving force, these studies are not definitive since surface charge and adsorption are very well-correlated for all these systems.

The present study illustrates that uracil, pyridine and 2,2'-bipyridine stabilize the reconstructed structure of Au(111) when the experiment is started at well-defined negative potentials. These findings are different from the effect of specifically adsorbed halide ions, which significantly decrease the stability of the Au(111)-($p \times \sqrt{3}$) surface [19,20]. We interpret these observations qualitatively in terms of the interplay between ordered adlayer-structures and specific adsorbate-substrate interactions, which determine the interfacial energetics and the mobility of the individual gold surface atoms.

The kinetic studies demonstrate that the reconstruction and lifting of the reconstruction follow nucleation-and-growth-based mechanisms. The lifting of the reconstruction in the presence of uracil proceeds in two steps, which involve the disintegration of the $p \times \sqrt{3}$ phase and the transformation of a disordered surface structure into an ordered (1×1) phase. The potential-induced reconstruction can be described by an Avrami-type formalism with exponents ranging between 1.9 and 2.3.

The comparison of our present results with related experimental findings supports a more general approach on the stability of the Au(*hkl*) faces in the presence of adsorbates: the adsorbates alone do not necessarily lift the reconstruction of Au(*hkl*). Our new experimental findings showed that the Au(111) surface reconstruction is (kinetically) stable in the presence of uracil, pyridine or 2,2'-bipyridine. Similarly, the hexagonal reconstruction of the Au(100) surface is stable in the presence of CO, formaldehyde and glucose [38]. In contrast, the reduction of the stability range of Au(100)-(hex) was documented for pyridine, pyrazine and thiourea [39]. Halides are also well known to lift the reconstruction, even though small halide coverages (less than 5%) have probably no effect on the local and global reconstruction of the Au(111) surface [19]. Interestingly, halides do not lift the reconstruction when coadsorbed with certain cations [40].

Together, these results indicate that only few adsorbates lift the reconstruction. Most probably the nature of the adsorbate-gold interaction and of the adsorbate-adsorbate interactions, as well as their effect on the free electron density, determine the structure of the gold surface.

Acknowledgements

The authors would like to acknowledge with great pleasure many very thoughtful and constructive discussions with J. Wang and D.M. Kolb. One of us (Th.W.) acknowledges the support of the Deutsche Forschungsgemeinschaft through a Heisenberg Fellowship. The research at Brookhaven National Laboratory was supported by the

Division of Materials and Chemical Sciences Research, US Department of Energy, under contract DE-AC02-76CH00016 and by a grant from the Natural Sciences and Engineering Research Council of Canada.

References

- [1] J.V. Barth, H. Brune, G. Ertl and R.J. Behm, *Phys. Rev. B*, 42 (1990) 9307.
- [2] D. Gibbs, B.M. Ocko, D.M. Zehner and S.G.J. Mochrie, *Phys. Rev. B*, 42 (1990) 7330.
- [3] E. Vlieg, I.K. Robinson and K. Kern, *Surf. Sci.*, 233 (1990) 248.
- [4] A.R. Sandy, S.G.J. Mochrie, D.M. Zehner, K.G. Huang and D. Gibbs, *Phys. Rev. B*, 43 (1991) 4667.
- [5] A. Hamelin, *J. Electroanal. Chem.*, 142 (1982) 299.
- [6] D.M. Kolb, G. Lehmpfuhl and M.S. Zei, *J. Electroanal. Chem.*, 179 (1984) 289.
- [7] D.M. Kolb and J. Schneider, *Electrochim. Acta*, 31 (1986) 929.
- [8] M.S. Zei, G. Lehmpfuhl and D.M. Kolb, *Surf. Sci.*, 221 (1986) 23.
- [9] D.M. Kolb and J. Schneider, *Surf. Sci.*, 162 (1985) 764.
- [10] B.M. Ocko, J. Wang, A. Davenport and H. Isaacs, *Phys. Rev. Lett.*, 65 (1990) 1466.
- [11] B.M. Ocko, G. Helgessen, B. Schardt and J. Wang, *Phys. Rev. Lett.*, 69 (1992) 3350.
- [12] X. Gao, A. Hamelin and M.J. Weaver, *Phys. Rev. B*, 44 (1991) 10983.
- [13] X. Gao, A. Hamelin, M.J. Weaver, *Phys. Rev. B*, 46 (1992) 7096.
- [14] X. Gao, G.J. Eden, A. Hamelin and M.J. Weaver, *Surf. Sci.*, 296 (1993) 333.
- [15] N.J. Tao and S.M. Lindsay, *Surf. Sci. Lett.*, 274 (1992) L546.
- [16] O.M. Magnussen, J. Hotlos, R.J. Behm, N. Batina and D.M. Kolb, *Surf. Sci.*, 296 (1993) 310.
- [17] D.M. Kolb, A.S. Dakkouri and N. Batina, in A.A. Gewirth and H. Siegenthaler (Eds.), *Nanoscale Probes of the Solid/Liquid Interface*, NATO ASI, Serie C, Vol. 288, Kluwer, Dordrecht, 1995, p. 263.
- [18] I.M. Tidswell, N.M. Markovic and P.N. Ross, *Surf. Sci.*, 317 (1994) 241.
- [19] J. Wang, B.M. Ocko, A.J. Davenport and H.S. Isaacs, *Phys. Rev. B*, 46 (1992) 10321.
- [20] J. Wang, A.J. Davenport, H.S. Isaacs and B.M. Ocko, *Science*, 255 (1992) 1416.
- [21] A. Friedrich, B. Pettinger, D.M. Kolb, G. Lüpke, R. Steinhoff and G. Marowsky, *Chem. Phys. Lett.*, 163 (1989) 123.
- [22] D.J. Trevor, C.E.D. Chidsey and D.N. Loicongo, *Phys. Rev. Lett.*, 62 (1989) 929.
- [23] J. Hageböck, MS Thesis, Department of Physics, Ludwig-Maximilian University, Munich, 1992.
- [24] M. Hölzle, T. Wandlowski and D.M. Kolb, *Surf. Sci.*, 335 (1995) 281.
- [25] D. Dickertmann, F.D. Koppitz and J.W. Schultze, *Electrochim. Acta*, 21 (1976) 967.
- [26] A. Dakkouri, T. Wandlowski and D.M. Kolb, in preparation.
- [27] W. Saenger, *Principles of Nucleic Acid Structure*, Springer, Berlin, 1984, Chapter 8.
- [28] J.M. Dona and J. Gonzalez-Velasco, *Surf. Sci.*, 274 (1992) 205.
- [29] M. Avrami, *J. Chem. Phys.*, 7 (1939) 1103; *J. Chem. Phys.*, 8 (1940) 212.
- [30] R. de Levie, in H. Gerischer (Ed.), *Advances in Electrochemistry and Electrochemical Engineering*, Vol. 13, Wiley-Interscience, New York, 1985, p. 1.
- [31] L. Stollberg, S. Morin, J. Lipkowski and D.E. Irish, *J. Electroanal. Chem.*, 307 (1991) 241.
- [32] D. Yang, D. Bizotto, J. Lipkowski, B. Pettinger and S. Mirwald, *J. Phys. Chem.*, 98 (1994) 7083.

- [33] T. Wandlowski, M. Hölzle and D.M. Kolb, in preparation.
- [34] F. Sette, T. Hashizume, F. Comin, A.A. MacDowell and P. Citrin, *Phys. Rev. Lett.*, 61 (1988) 1384.
- [35] B.M. Ocko, O.M. Magnussen, R.R. Adzic, J.X. Wang, Z. Shi and J. Lipkowski, *J. Electroanal. Chem.*, 376 (1994) 1384.
- [36] C.N. van Huong, C. Hinnen and J. Rousseau, *J. Electroanal. Chem.*, 151 (1983) 149.
- [37] C. Alonso, R.C. Salvarezza, J.M. Vara and A.J. Arvia, *Electrochim. Acta*, 35 (1990) 1331.
- [38] R.R. Adzic, J.X. Wang, O.M. Magnussen and B.M. Ocko, *Langmuir*, 12 (1996) 513.
- [39] U.W. Hamm and D.M. Kolb, *J. Electroanal. Chem.*, 332 (1992) 339.
- [40] Th. Wandlowski, unpublished results, 1995.